

## A Density Functional Theory Investigation of the Fragmentation Mechanism of Deprotonated $\alpha$ -Alanine

Quan Sun<sup>1\*</sup>, Hongjie Qu<sup>1</sup>, Qiang Li<sup>1</sup>, Dongxue Ding<sup>1</sup>, Lili Cao<sup>1</sup>, Jingyu Pang<sup>1</sup>

<sup>1</sup>College of Science, Heilongjiang Bayi Agricultural University, Daqing, 163319, Heilongjiang Province, P. R. China

DOI: [10.36347/sjet.2022.v10i07.005](https://doi.org/10.36347/sjet.2022.v10i07.005)

| Received: 11.06.2022 | Accepted: 17.07.2022 | Published: 20.07.2022

\*Corresponding author: Quan Sun

College of Science, Heilongjiang Bayi Agricultural University, Daqing, 163319, Heilongjiang Province, P. R. China

### Abstract

### Review Article

In this paper, density functional theory (DFT) was applied to study the isomerization process and fragmentation mechanism of deprotonated  $\alpha$ -alanine ions ( $[\alpha\text{-Ala-H}]^-$ ) at B3LYP/6-311++G(2df,2pd) level. Taking **a2**, the lowest energy of the  $[\alpha\text{-Ala-H}]^-$  isomers as the zero point, the potential energy profiles of the  $[\alpha\text{-Ala-H}]^-$  in isomerization, H<sub>2</sub>O- and NH<sub>3</sub>-loss reaction pathways were plotted using Relative Gibbs free Energies (R.G.) relative to **a2** as the reference point. In the isomerization process, the reaction barrier ( $\Delta G^\ddagger$ ) required for hydrogen transfer is higher than other ones. From the perspective of chemical reaction thermodynamics, **Path 11** of deamination to **p3** is the only positive spontaneous pathway among all H<sub>2</sub>O- and NH<sub>3</sub>-loss pathways; and from the perspective of reaction kinetics, the dominant path is **Path 2** of H<sub>2</sub>O-loss pathways ( $\Delta G_{\text{TS9}}^\ddagger = 53.65 \text{ kcal}\cdot\text{mol}^{-1}$ ). In addition, the effect of temperature on reaction pathways and dissociative products were also investigated. The results show that temperature has little effect on H<sub>2</sub>O- and NH<sub>3</sub>-loss pathways.

**Keywords:** deprotonated  $\alpha$ -alanine ions, reaction mechanism, H<sub>2</sub>O-loss pathways, NH<sub>3</sub>-loss pathways.

**Copyright © 2022 The Author(s):** This is an open-access article distributed under the terms of the Creative Commons Attribution 4.0 International License (CC BY-NC 4.0) which permits unrestricted use, distribution, and reproduction in any medium for non-commercial use provided the original author and source are credited.

## 1. INTRODUCTION

Alpha-amino acids are one of nature's most important building blocks and are also thought to play a key role in interstellar chemistry and the origin of life on Earth [1, 2].  $\alpha$ -alanine is one of the simplest amino acids, which can be obtained by the removal of CO<sub>2</sub> from aspartic acid catalyzed by enzyme [3].  $\alpha$ -alanine is a non-essential amino acid in human body, but it has significant significance in asymmetric synthesis [6], functional material synthesis [7], pharmaceutical science [8-10] and interstellar exploration [11].

In 1993, Godfrey [12] and Attila *et al.*, [13] determined the gas phase structure of  $\alpha$ -alanine experimentally [12] and theoretically [13] respectively. Subsequently, Iijima [14, 15] and Attila [16] determined the position of heavy atoms in the most stable structure of  $\alpha$ -alanine gas phase from experiment [14, 15] and theory [16] respectively. The structure of  $\alpha$ -alanine in aqueous solution is zwitterionic [17, 18],

the crystal space group is P2<sub>1</sub>2<sub>1</sub>2<sub>1</sub>, and the unit-cell dimensions are  $a = 6.032$ ,  $b = 12.343$ ,  $c = 5.784 \text{ \AA}$  [19].

Eckersley [20] obtained dehydrated and deaminated proton-alanine fragments by fast atomic bombardment mass spectrometry (FAB-MS/MS), but Choi [21] did not obtain corresponding fragments by atmospheric pressure chemical ionization mass spectrometry (APCI-MS), and the fragmentation mechanism is unknown.

Based on the investigation of the fragmentation mechanism of deprotonated asparagine [22], the geometric configurations of the reactants, intermediates, transition states, product ions and neutral molecules of deprotonated  $[\alpha\text{-Ala-H}]^-$  were optimized, the thermodynamic data were obtained by frequency analysis. The potential energy profiles of isomerization, H<sub>2</sub>O- and NH<sub>3</sub>-loss pathways of  $[\alpha\text{-Ala-H}]^-$  were constructed respectively, and then judge the dominant

pathway and the dominant product. In addition, the influence of temperature on H<sub>2</sub>O- and NH<sub>3</sub>-loss pathways, and dominant product were also analyzed in this study. The results will provide some model support for clarifying the fragmentation mechanism of deprotonated amino acid ions.

## 2. COMPUTATIONAL DETAILS

Since the *S*- and *R*- structures of  $\alpha$ -alanine are mirror symmetric, only the *S*- chirality of  $\alpha$ -alanine is selected as the investigated target in this study. The geometric configurations of all reactants, intermediates, transition states, products and dissociated neutral molecules were obtained by using B3LYP method [23-25] combined with 6-311++G(2df,2pd) base set [26] in incorporated in the Gaussian09 program system [27]. After geometric optimization, frequency vibration calculation is carried out to determine the geometrical position is the minimum value (no virtual frequency) or

transition state (only one virtual frequency). In addition, we also calculate the thermal correction of the key stability points at the same level in geometric optimization, and obtain their relative enthalpy of reaction and Gibbs free energy of relative reaction with temperature.

## 3. RESULT AND DISCUSSION

### 3.1 Isomerization of [ $\alpha$ -Ala-H]<sup>-</sup>

In this study, 23 isomers of [ $\alpha$ -Ala-H]<sup>-</sup> were calculated, which could be divided into 5 groups according to the position of negative charge, whether the molecule formed a ring, and the *cis-trans* isomerism of the ring formed molecule. The relative electron total energies (R.E.), relative enthalpies (R.H.) and relative Gibbs-free energies (R.G.) are all took **a2**, the lowest energy isomer, as reference point, and the relevant data are listed in Table 1.

**Table 1: Total Energies (TE, *a.u.*), Zero-point Energies (ZPE, *a.u.*), Relative Total Energies (R.E., kcal·mol<sup>-1</sup>), Enthalpies (H, *a.u.*), Relative Enthalpies (R.H., kcal·mol<sup>-1</sup>), Gibbs-free Energies (G, *a.u.*) and Relative Gibbs-free Enthalpies (R.G., kcal·mol<sup>-1</sup>) of [ $\alpha$ -Ala-H]<sup>-</sup>**

Species	TE	ZPE	TE+ZPE	R.E.	H	R.H.	G	R.G.
<b>a1</b>	-323.320856	0.094320	-323.226536	0.04	-323.210710	0.02	-323.281392	0.25
<b>a2</b>	-323.320718	0.094119	-323.226599	0.00	-323.210739	0.00	-323.281785	0.00
<b>b1</b>	-323.276896	0.092121	-323.184775	26.24	-323.167927	26.86	-323.239945	26.25
<b>b2</b>	-323.268887	0.091499	-323.177388	30.88	-323.160228	31.70	-323.233867	30.07
<b>b3</b>	-323.275272	0.091880	-323.183392	27.11	-323.166351	27.85	-323.239320	26.65
<b>b4</b>	-323.269382	0.091520	-323.177862	30.58	-323.160960	31.24	-323.233128	30.53
<b>b5</b>	-323.276316	0.092224	-323.184092	26.67	-323.167776	26.96	-323.238726	27.02
<b>b6</b>	-323.260121	0.090703	-323.169418	35.88	-323.152111	36.79	-323.226570	34.65
<b>b7</b>	-323.268890	0.091363	-323.177527	30.79	-323.160555	31.49	-323.232857	30.70
<b>b8</b>	-323.271165	0.091753	-323.179412	29.61	-323.162660	30.17	-323.234350	29.77
<b>c1</b>	-323.232988	0.091981	-323.141007	53.71	-323.124391	54.18	-323.195378	54.22
<b>c2</b>	-323.231857	0.091776	-323.140081	54.29	-323.123339	54.84	-323.194645	54.68
<b>c3</b>	-323.227501	0.091373	-323.136128	56.77	-323.119319	57.37	-323.190950	57.00
<b>c4</b>	-323.227188	0.090737	-323.136451	56.57	-323.119285	57.39	-323.191647	56.56
<b>c5</b>	-323.240135	0.092278	-323.147857	49.41	-323.131765	49.56	-323.201540	50.35
<b>c6</b>	-323.226990	0.090703	-323.136287	56.67	-323.119144	57.48	-323.191329	56.76
<b>c7</b>	-323.224230	0.091177	-323.133053	58.70	-323.116361	59.22	-323.187995	58.85
<b>c8</b>	-323.228883	0.091569	-323.137314	56.03	-323.120595	56.57	-323.191933	56.38
<b>d1</b>	-323.229516	0.092084	-323.137432	55.95	-323.121146	56.22	-323.190969	56.99
<b>d2</b>	-323.232361	0.092322	-323.140039	54.32	-323.124002	54.43	-323.192922	55.76
<b>e1</b>	-323.226467	0.091917	-323.134550	57.76	-323.118034	58.17	-323.188653	58.44
<b>e2</b>	-323.228696	0.092222	-323.136474	56.55	-323.120384	56.70	-323.189262	58.06
<b>e3</b>	-323.218768	0.091985	-323.126783	62.64	-323.110821	62.70	-323.179362	64.27

Among them, species **a** has the lowest energy whose negative charge is located on CO<sub>2</sub> (R.G. ranges from 0.00 ~ 0.25 kcal·mol<sup>-1</sup>); species **b** has a relatively high energy and the negative charge at  $\alpha$ -C (26.25 ~ 34.65 kcal·mol<sup>-1</sup>); and the energies of **c**, **d** and **e** anions are the highest, and the energies of these three anions are similar to each other (50.35 ~ 64.27 kcal·mol<sup>-1</sup>). The difference between **c**, **d** and **e** lies in that the negative charge of **c** anion is on  $\beta$ -C, while the negative charge of **d** and **e** anion is on O atom, but **d** and **e** are *cis-trans* isomerism.

Figure 1 shows the isomerization potential energy profiles between the 23 isomers. As can be seen from the figure, the isomerization of [ $\alpha$ -Ala-H]<sup>-</sup> underwent three hydrogen transfers. The first of which was **a2** passing through the transition state **TS22** to **b2**, while the negative charge was transferred from CO<sub>2</sub> to  $\alpha$ -C. In the second and third steps, **b1** goes through the transition state **TS24** to **c6**, and **b3** goes through the transition state **TS23** to **c2**, respectively. In these two steps, the negative charge is transferred from  $\alpha$ -C to  $\beta$ -C. After that, the isomerization from species **c** to **d** and **e**

is that **c6** goes through the transition state **TS25** to **e1**, and **c4** goes through the transition state **TS17** to **d1**, respectively. In both cases, there has a new  $\sigma$  bond

formed between the carboxyl carbon and  $\beta$ -C, and the negative charge ends up on the carboxyl oxygen.

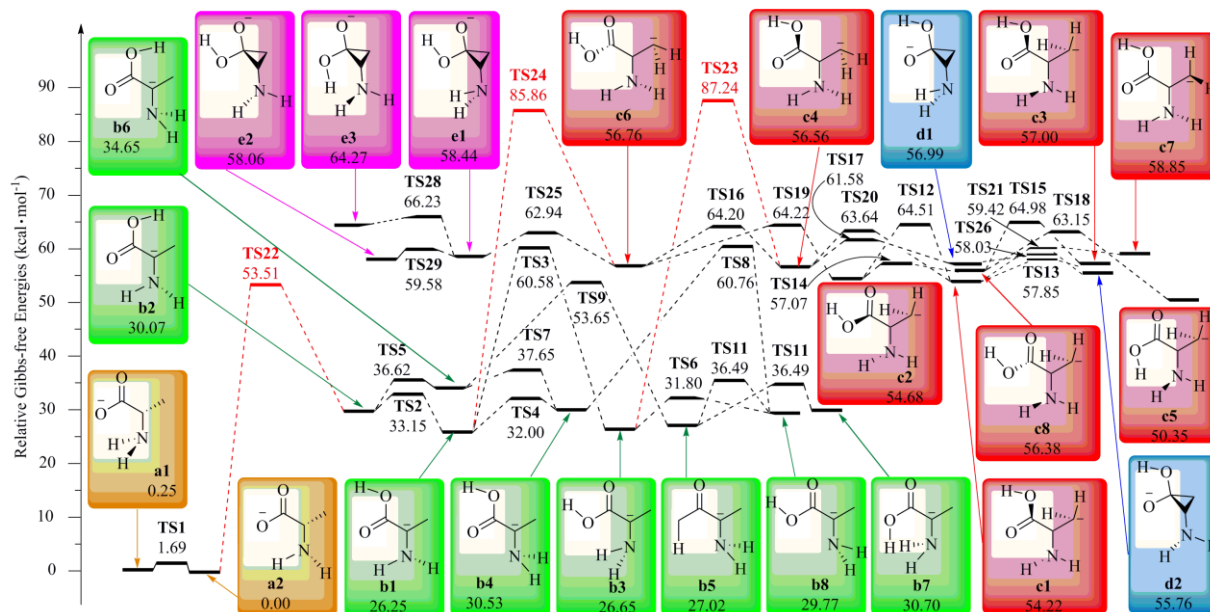


Figure 1: Isomerization potential energy profile of  $[\alpha\text{-Ala-H}]^-$  computed at the B3LYP/6-311++G(2df,2pd) level of theory with the temperature of 473.15 K

Figure 1 shows that the isomerization barriers ( $\Delta G^\ddagger$ ) required for  $\sigma$  bond rotation between similar molecules is less than 8 kcal·mol<sup>-1</sup>, while the barriers ( $\Delta G^\ddagger$ ) required for hydrogen transfer is more than 50 kcal·mol<sup>-1</sup>. Among them, there are three special isomerization steps between the same molecule required reaction potential barriers ( $\Delta G^\ddagger$ ) between 19 ~ 35 kcal·mol<sup>-1</sup>, which is due to the negative charge of **b** anion in  $\alpha$ -C, which makes the oxygen atom combined with carboxyl carbon by double bond, carboxyl carbon atom and  $\alpha$ -C anion form conjugated structure. As a

result, a chemical bond between the carboxyl carbon and  $\alpha$ -C is formed, which is between single and double bonds.

### 3.2 H<sub>2</sub>O-loss reaction of $[\alpha\text{-Ala-H}]^-$

The potential energy profile of H<sub>2</sub>O-loss pathways of  $[\alpha\text{-Ala-H}]^-$  were shown in figure 2. All the energies given in the figure are relative Gibbs free energies (R.G., kcal·mol<sup>-1</sup>) obtained with **a2** as reference point.

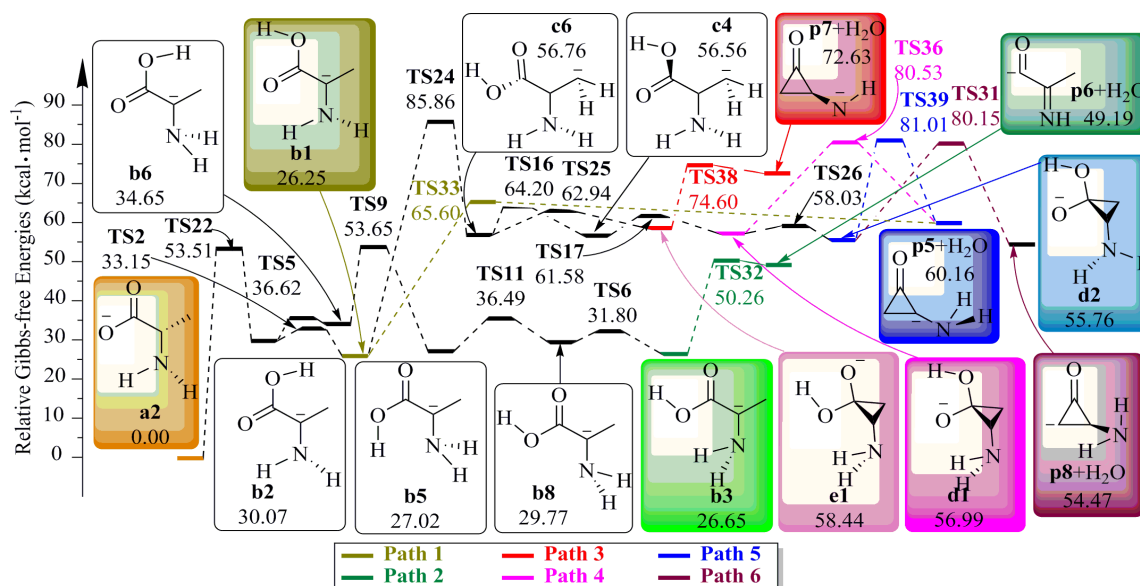


Figure 2: Potential energy profile of H<sub>2</sub>O-loss fragmentation reaction computed at the B3LYP/6-311++G(2df,2pd) level of theory with the temperature of 473.15 K

As can be seen from Figure 2, the initial reactant **a2** undergoes a series of isomerization processes to the isomers **b1**, **b3**, **d1**, **d2** and **e1** that can directly undergo pyrolysis reaction. The resulting products after dehydration are **p5**, **p6**, **p7** and **p8**, respectively. **Path 1**, **Path 3** and **Path 5** were corresponding to the same product, and the reactant **d2** was dehydrated in two different ways, resulting in two different products **p5** and **p8** respectively. From the perspective of reaction thermodynamics, the reaction Gibbs-free energies ( $\Delta_rG$ ) of **Path 1** to **Path 6** is greater than 0, indicating that the six reaction paths are all forward non-spontaneous reactions. Among the four products, **p6** has the lowest energy and is the dominant product. From the perspective of reaction kinetics, **Path**

**2** has a relatively low barrier ( $\Delta G_{TS9}^\ddagger = 53.65 \text{ kcal}\cdot\text{mol}^{-1}$ ), which is more advantageous than other  $\text{H}_2\text{O}$ -loss pathways. Therefore, **Path 2** is the dominant pathway in the  $\text{H}_2\text{O}$ -loss reaction of  $[\alpha\text{-Ala-H}]^-$ , and the corresponding product **p6** was also the dominant product in the dehydration products.

### 3.3 $\text{NH}_3$ -loss reaction of $[\alpha\text{-Ala-H}]^-$

The potential energy profile of  $\text{NH}_3$ -loss pathways of  $[\alpha\text{-Ala-H}]^-$  were shown in Figure 3. All the energies given in the figure are relative Gibbs free energies (R.G.,  $\text{kcal}\cdot\text{mol}^{-1}$ ) obtained with **a2** as reference point.

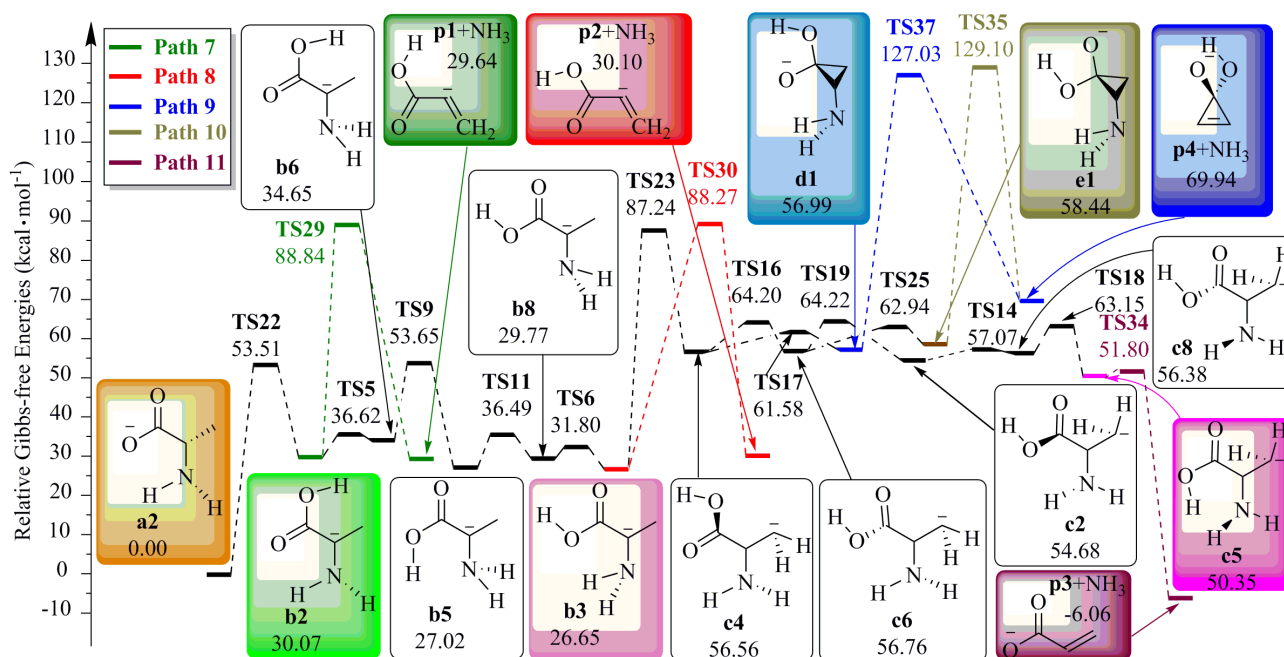


**Figure 3:** Potential energy profile of  $\text{NH}_3$ -loss fragmentation reaction computed at the B3LYP/6-311++G(2df,2pd) level of theory with the temperature of 473.15 K

It can be seen from the five response pathways that the decisive steps of **Paths 7 ~ 11** are **TS29**, **TS30**, **TS37**, **TS35** and **TS23** respectively. From the perspective of reaction thermodynamics, only reaction Gibbs-free energy ( $\Delta_rG$ ) of **Path 11** is less than 0 among the five reaction paths, and the other reactions are all positive non-spontaneous reactions, and product **p3** is also the dominant product among all the deamination products. From the perspective of reaction kinetics, **Paths 9 ~ 10** have the highest reaction barriers ( $\Delta G^\ddagger$ ), **Path 7**, **Path 8** and **Path 11** have lower reaction barriers and were close to each other ( $\Delta G_{TS29}^\ddagger = 88.84 \text{ kcal}\cdot\text{mol}^{-1}$ ,  $\Delta G_{TS30}^\ddagger = 88.27 \text{ kcal}\cdot\text{mol}^{-1}$ ,  $\Delta G_{TS23}^\ddagger = 87.24 \text{ kcal}\cdot\text{mol}^{-1}$ ). **Path 11** was the most dominant pathway among the five  $\text{NH}_3$ -loss pathways of  $[\alpha\text{-Ala-H}]^-$ .

### 3.4 Temperature dependence of the $\text{H}_2\text{O}$ - and $\text{NH}_3$ -loss reaction

In order to investigate the influence of temperature on the reaction pathways and products, the reference point **a2**, the transition states of the rate-determining steps in the reaction pathways and transition states that are close to the energy of the rate-determining steps, the products after dehydration and deamination, and two neutral molecules,  $\text{NH}_3$  and  $\text{H}_2\text{O}$ , were selected for frequency analysis and calculated the thermodynamic data. The selected temperature range is 273.15 ~ 853.15K, and the interval temperature is 20 K. The results are shown in Figure 4.

Figure 4 shows the curves of energy variation with temperature (the temperature ranges is 273.15 ~ 853.15 K, with an interval of 20 K) of all possible rate-determination steps (the transition state in which the difference of Gibbs-free energy is less than 2  $\text{kcal}\cdot\text{mol}^{-1}$

<sup>1</sup>) of H<sub>2</sub>O- and NH<sub>3</sub>-loss pathways. Figure 4(a) shows the curves of rate-determination steps of H<sub>2</sub>O-loss pathways with temperature change, and Figure 4(b) shows the curves of rate-determination steps of NH<sub>3</sub>-

loss pathways with temperature change. As can be seen from the figure, the influence of temperature on each H<sub>2</sub>O- and NH<sub>3</sub>-loss pathways of [ $\alpha$ -Ala-H]<sup>-</sup> is basically controlled within 5 kcal·mol<sup>-1</sup>.

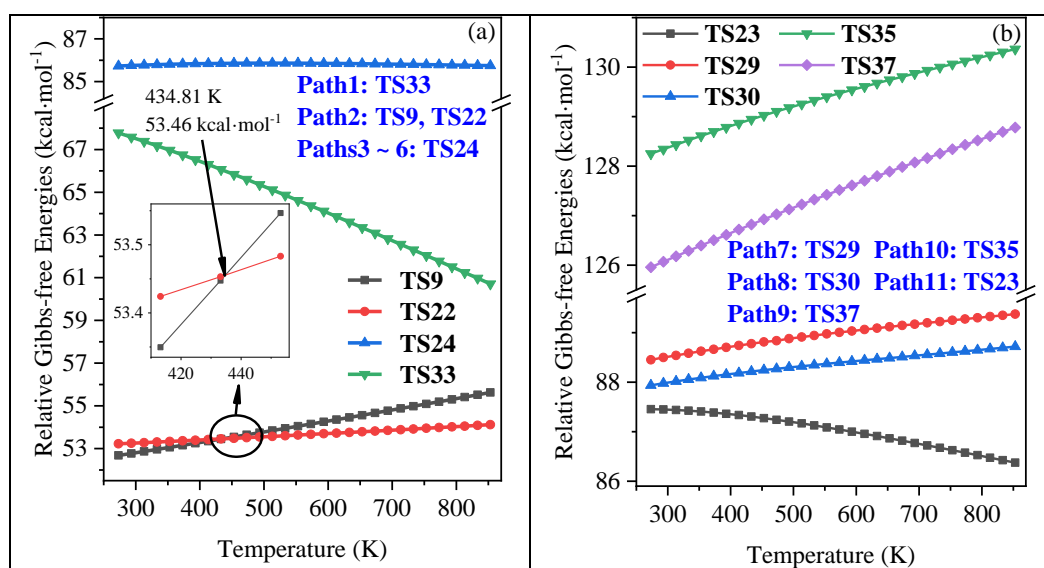


**Figure 4: Temperature dependence of the rate-determining steps for the H<sub>2</sub>O- (a) and NH<sub>3</sub>-loss (b) reactions computed at the B3LYP/6-311++G(2df,2pd) level of theory**

As shown in Figure 4(a), the rate-determining steps of H<sub>2</sub>O-loss pathways **Paths 3 ~ 6** is **TS24**, whose energy is basically unchanged with the increase of temperature. Rate-determining step of **Path 1** is **TS33**, whose energy changes 7.06 kcal·mol<sup>-1</sup> with the temperature ranges from 273.15 K to 853.15 K, which is the largest energy change among the six H<sub>2</sub>O-loss pathways and the sole rate-determining step whose energy changes exceed 5 kcal·mol<sup>-1</sup> among all the reaction pathways. **TS9** and **TS22** are two possible rate-determination steps for **Path 2** because they have very similar energies. As can be seen from the figure, when the temperature is lower than 434.81 K, **TS22** is the rate-determining step of **Path 2**; when the temperature is higher than 434.81 K, **TS29** becomes the rate-determining step; and the reaction barrier ( $\Delta G^\ddagger$ ) of H<sub>2</sub>O-loss reaction is 53.46 kcal·mol<sup>-1</sup> at 434.81 K. Therefore, **Path 2** is always the optimal path for H<sub>2</sub>O-

loss pathways when the temperature is controlled within 273.15 ~ 853.15 K.

Figure 4(b) shows the curve of the rate-determining step of the NH<sub>3</sub>-loss pathways changing with temperature. As can be seen from this figure, **Paths 9 ~ 10** are the two reaction pathways with the highest reaction barriers among all the NH<sub>3</sub>-loss pathways. Among the five NH<sub>3</sub>-loss pathways, only the reaction barrier of **Path 11** rate-determining step decreased with the increasing temperature, while the reaction barriers of the other four NH<sub>3</sub>-loss pathways increased with the increasing temperature. The reaction barriers of **Paths 9 ~ 10** are increased significantly than that of **Paths 7 ~ 8**, but the barriers variation range was controlled within 3 kcal·mol<sup>-1</sup>. It can be seen that **Path 11** is always the optimal pathway in all the NH<sub>3</sub>-loss pathways with the temperature ranged from 273.15 to 853.15K.

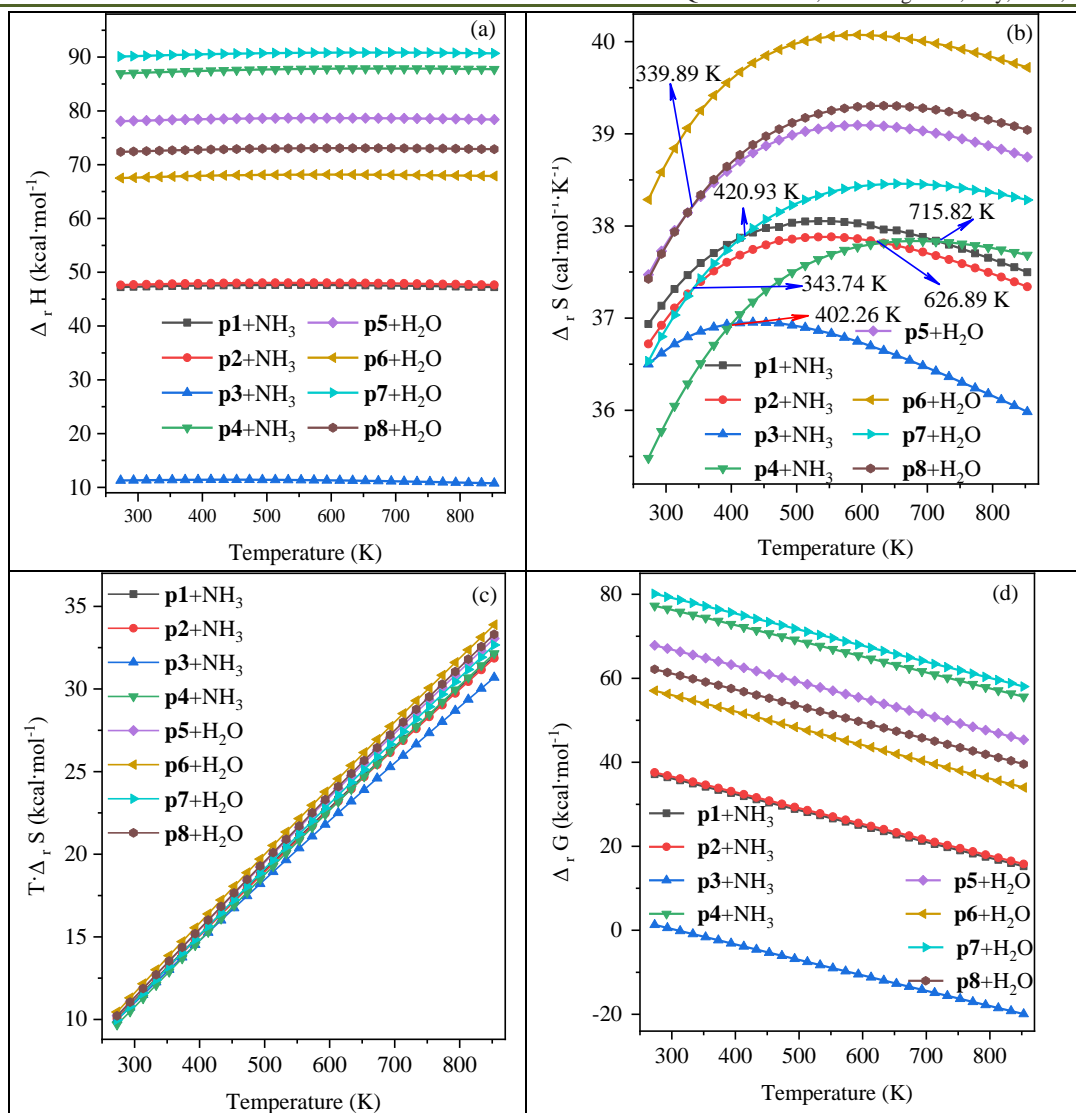


**Figure 5: Temperature dependence of the reaction enthalpies ( $\Delta_r H$ ) (a), reaction entropies ( $\Delta_r S$ ) (b),  $T \cdot \Delta_r S$  (c), and reaction Gibbs free energies ( $\Delta_r G$ ) (d) for the fragmentation reactions starting from reactant a2 computed at the B3LYP/6-311++G(2df,2pd) level of theory**

Figure 5 shows the thermodynamic data variation curves of four H<sub>2</sub>O-loss products and four NH<sub>3</sub>-loss products with the increasing temperature. It can be seen from Figure 5(a) that the reaction enthalpies ( $\Delta_r H$ ) of the NH<sub>3</sub>-loss products is lower than that of the H<sub>2</sub>O-loss products, while **p3** is the most dominant product among all the H<sub>2</sub>O-loss and NH<sub>3</sub>-loss products, and the  $\Delta_r H$  of all products changes very little with the increasing temperature. As shown in Figure 5(b), their appears energy interleaving with the increasing temperature among the reaction entropy ( $\Delta_r S$ ) of different reactants, however, all  $\Delta_r S$  vary within 2 cal·mol<sup>-1</sup>·K<sup>-1</sup> in the temperature range of 273.15 ~ 853.15 K. Figure 5(c) shows a significant linear increase in  $T \cdot \Delta_r S$  for different reactants, which is affected by temperature rather than  $\Delta_r S$ . It can be seen from Figure 5(d) that  $\Delta_r G$  of all reactants decreases linearly with the increasing temperature. Relative Gibbs-free energies of H<sub>2</sub>O-loss products are higher than that of NH<sub>3</sub>-loss products, and NH<sub>3</sub>-loss product

**p3** is still the most dominant product in thermodynamics.

#### 4. CONCLUSION

The reaction mechanism of [ $\alpha$ -Ala-H]<sup>-</sup> at B3LYP/6-311++G(2df,2pd) level with the temperature of 473.15 K shows that H<sub>2</sub>O- and NH<sub>3</sub>-loss reaction could be realized when the energy provided by the environment was higher than 87.24 kcal·mol<sup>-1</sup>. The details are listed below.

1. In the process of isomerization of [ $\alpha$ -Ala-H]<sup>-</sup>, the reaction barriers ( $\Delta G^\ddagger$ ) required for hydrogen transfer is the highest; and the carboxyl rotation of **b** is affected by conjugation, whose  $\Delta G^\ddagger$  is higher than that of other  $\sigma$  bond rotations. The  $\Delta G^\ddagger$  is basically within 3 kcal·mol<sup>-1</sup> for  $\sigma$  bond rotation and isomerization among **c**, **d** and **e**.
2. The dominant H<sub>2</sub>O-loss pathway of [ $\alpha$ -Ala-H]<sup>-</sup> is **Path 2**, and the corresponding product **p6** is also the dominant product. The dominant NH<sub>3</sub>-loss

pathway of  $[\alpha\text{-Ala-H}]^-$  is **Path 11**, and the corresponding product **p3** is also the dominant product. From the perspective of thermodynamics, the reaction pathway **Path 11** corresponding to  $\text{NH}_3$ -loss product **p3** is the unique reaction pathway that can proceed spontaneously in the forward direction, and **p3** is also the most dominant product in all the  $\text{H}_2\text{O}$ - and  $\text{H}_2\text{O}$ -loss pathways. However, from the perspective of reaction kinetics, the  $\Delta G^\ddagger$  of  $\text{H}_2\text{O}$ -loss pathway **Path 2** is the lowest, which is the most dominant reaction pathway among all the reaction pathways.

- It is investigated that only the rate-determine step of **Path 2** changed with the temperature increasing (273.15 K  $\sim$  573.15 K), while the dominant pathway of all  $\text{H}_2\text{O}$ - and  $\text{NH}_3$ -loss reaction did not change, and the corresponding dominant products did not change either.

**Fund project:** “Three Longitudinal” Youth Innovative Talent Project of Heilongjiang Bayi Agricultural University (ZRCQC202010); Daqing City guiding science and technology project (zd-2021-88); Doctoral Research Foundation of Heilongjiang Bayi Agricultural University (XDB202112)

**Author’s brief introduction:** Quan Sun (1990-), man, Master’s Degree, Assistant laboratory Technician, Corresponding author, mainly engaged in theoretical study on the reaction mechanism of substances.

## REFERENCE

- Brack, A. (Ed.). (1998). *The molecular origins of life: assembling pieces of the puzzle*. Cambridge University Press.
- Nelson, G., Chandrashekar, J., Hoon, M. A., Feng, L., Zhao, G., Ryba, N. J., & Zuker, C. S. (2002). An amino-acid taste receptor. *Nature*, *416*(6877), 199-202.
- Meister, A., Sober, H. A., & Tice, S. V. (1951). Enzymatic decarboxylation of aspartic acid to  $\alpha$ -alanine. *Journal of Biological Chemistry*, *189*, 577-590.
- Rezaei, R., Wang, W., Wu, Z., Dai, Z., Wang, J., & Wu, G. (2013). Biochemical and physiological bases for utilization of dietary amino acids by young pigs. *Journal of animal science and biotechnology*, *4*(1), 1-12.
- Rezaei, R., Wu, Z., Hou, Y., Bazer, F. W., & Wu, G. (2016). Amino acids and mammary gland development: nutritional implications for milk production and neonatal growth. *Journal of animal science and biotechnology*, *7*(1), 1-22.
- Qiu, W., Soloshonok, V. A., Cai, C., Tang, X., & Hruby, V. J. (2000). Convenient, large-scale asymmetric synthesis of enantiomerically pure trans-cinnamylglycine and  $\alpha$ -alanine. *Tetrahedron*, *56*(17), 2577-2582.
- Hong, J., Zhu, Z., Lu, H., & Qiu, Y. (2014). Synthesis and arsenic adsorption performances of ferric-based layered double hydroxide with  $\alpha$ -alanine intercalation. *Chemical Engineering Journal*, *252*, 267-274.
- Sun, T., & Xu, Z. (2006). Radical scavenging activities of  $\alpha$ -alanine C60 adduct. *Bioorganic & medicinal chemistry letters*, *16*(14), 3731-3734.
- Koshkin, S. A., Garifzyanov, A. R., Davletshina, N. V., Kataeva, O. N., Islamov, D. R., & Cherkasov, R. A. (2015). Synthesis of new lipophilic phosphine oxide derivatives of natural amino acids and their membrane transport properties toward carboxylic acids. *Russian Journal of Organic Chemistry*, *51*(9), 1232-1244.
- Liu, J., Jiang, C., Liu, F., Gao, F., Zhang, X., Lei, Z., ... & Wang, Z. (2021). Theoretical study on the optical isomerization of  $\alpha$ -alanine Mn (II) complex in water-liquid phase environment. *Journal of ZheJiang University (Science Edition)*, *48*(6), 700-710.
- Moore, B., Toh, S. Y., Wong, Y. A., Bashiri, T., McKinnon, A., Wai, Y., ... & Momose, T. (2021). Hydrocarboxyl Radical as a Product of  $\alpha$ -Alanine Ultraviolet Photolysis. *The Journal of Physical Chemistry Letters*, *12*(50), 11992-11997.
- Godfrey, P. D., Firth, S., Hatherley, L. D., Brown, R. D., & Pierlot, A. P. (1993). Millimeter-wave spectroscopy of biomolecules: alanine. *Journal of the American Chemical Society*, *115*(21), 9687-9691.
- Csaszar, A. G. (1996). Conformers of gaseous  $\alpha$ -alanine. *The Journal of Physical Chemistry*, *100*(9), 3541-3551.
- Iijima, K., Tanaka, K., & Onuma, S. (1991). Main conformer of gaseous glycine: molecular structure and rotational barrier from electron diffraction data and rotational constants. *Journal of molecular structure*, *246*(3-4), 257-266.
- Iijima, K., & Beagley, B. (1991). An electron diffraction study of gaseous  $\alpha$ -alanine,  $\text{NH}_2\text{CH}_2\text{CH}_2\text{CO}_2\text{H}$ . *Journal of molecular structure*, *248*(1-2), 133-142.
- Császár, A. G. (1995). On the structures of free glycine and  $\alpha$ -alanine. *Journal of molecular structure*, *346*, 141-152.
- Zagórski, Z. P., & Sehested, K. (1998). Transients and stable radical from the deamination of  $\alpha$ -alanine. *Journal of radioanalytical and nuclear chemistry*, *232*(1), 139-141.
- Lu, Y., Bai, T., Xie, W., & Lu, J. (1998). The enthalpic interaction of  $\alpha$ -alanine with alkali metal halides in water at 298.15 K. *Thermochimica acta*, *319*(1-2), 11-15.
- Simpson, H. J., & Marsh, R. E. (1966). The crystal structure of L-alanine. *Acta Crystallographica*, *20*(4), 550-555.
- Eckersley, M., Bowie, J. H., & Hayes, R. N. (1989). Collision-induced dissociations of deprotonated  $\alpha$ -amino acids. The occurrence of specific proton transfers preceding fragmentation. *International journal of mass*

- spectrometry and ion processes*, 93(2), 199-213.
21. Choi, S. S., & Kim, O. B. (2013). Fragmentation of deprotonated amino acids in atmospheric pressure chemical ionization. *International Journal of Mass Spectrometry*, 338, 17-22.
  22. Sun, Q., & Yu, H. T. (2018). A density functional theory investigation of the fragmentation mechanism of deprotonated asparagine. *Computational and Theoretical Chemistry*, 1141, 45-52.
  23. Bak, K. L., Jørgensen, P., Helgaker, T., Ruud, K., & Jensen, H. J. R. A. (1993). Gauge-origin independent multiconfigurational self-consistent-field theory for vibrational circular dichroism. *The Journal of chemical physics*, 98(11), 8873-8887.
  24. Lee, C., Yang, W., & Parr, R. G. (1988). Development of the Colle-Salvetti correlation-energy formula into a functional of the electron density. *Physical review B*, 37(2), 785-789.
  25. Miehlich, B., Savin, A., Stoll, H., & Preuss, H. (1989). Results obtained with the correlation energy density functionals of Becke and Lee, Yang and Parr. *Chemical Physics Letters*, 157(3), 200-206.
  26. Frisch, M. J., Pople, J. A., & Binkley, J. S. (1984). Self-consistent molecular orbital methods 25. Supplementary functions for Gaussian basis sets. *The Journal of chemical physics*, 80(7), 3265-3269.
  27. Frisch, M. J., Trucks, G. W., Schlegel, H. B., Scuseria, G. E., Robb, M. A., Cheeseman, J. R., ... & Fox, D. J. (2009). Gaussian 09, Revision D. 01, Gaussian, Inc., Wallingford CT. *See also: URL: <http://www.gaussian.com>.*